# Next Generation Space Telescope: NIR InSb Array Development

Craig W. M<sup>c</sup>Murtry[a], William J. Forrest[a], Andrew C. Moore[a,b], and Judith L. Pipher[a]

[a]University of Rochester, Rochester, NY, USA
[b]Rochester Institute of Technology, Rochester, NY, USA

## ABSTRACT

The astronomical community has benefited from the scientific advances in photo-detection over the last few decades, from optical CCDs to infrared array detectors, for both large ground-based telescopes and space-borne telescopes. NGST, the successor to the Hubble Space Telescope, will draw on the improvements in infrared array technologies to achieve its goals and mission. The University of Rochester, in collaboration with Raytheon and NASA Ames Research Center, is developing and testing near infrared InSb array detectors to meet the stringent requirements for NGST. The latest development involves a suitable multiplexer in a $2048 \times 2048$ format that will be bump-bonded to an InSb array. Twenty of these arrays will be required for NGST imaging and spectroscopy. We present results for pathfinder $1024 \times 1024$ arrays. This is a companion work to the paper in these SPIE proceedings by Ken Ando, Peter Love, Nancy Lum, Alan Hoffman, Roger Holcombe, John Durkee, Joseph Rosbeck, and Elizabeth Corrales (Raytheon Infrared Operations).

**Keywords:** NIR, near infrared array detector, InSb, NGST, low noise

## 1. INTRODUCTION

The Infrared Astronomy group led by William Forrest and Judith Pipher at the University of Rochester is one of three independent detector testing laboratories for NASA's NGST.[1] The University of Rochester has achieved low noise, low dark current and high quantum efficiency, with good system electronics and optimized clocks and biases, using Raytheon produced high quality near infrared InSb array detectors which are ideal for space borne telescope missions, such as SIRTF.[2,3,4,5,6,7,8] We have chosen to work with Raytheon because InSb, on a suitably designed multiplexer, can meet or exceed all of the NGST requirements operating at a temperature of 30K. A detailed list of requirements and goals for NGST are provided by M<sup>c</sup>Creight et al.[9] The most relevant requirements and goals, as they pertain to this paper, include:

1. 48 Megapixels for imaging and 32 Megapixels for spectroscopy, with individual NIR arrays in $2048 \times 2048$ format,

2. Total noise per pixel in 1000 seconds multiply sampled integration, including dark current, is required to be below $9e^-$ with the goal of reaching $2.5e^-$,

3. Quantum efficiency requirement: $> 70\%$ for $0.6\mu m < \lambda < 1.0\mu m$ and $> 80\%$ for $1.0\mu m < \lambda < 5.0\mu m$ with goals of 90% and 95% respectively,

4. Well depth requirement: $> 6 \times 10^4 e^-$, goal: $> 2 \times 10^5 e^-$,

5. Pixel operability requirement: $> 98\%$, goal: $> 99.5\%$,

6. Operating temperature: $30K < T < 37K$,

7. Power dissipation requirement: $< 1mW$, goal: $< 100\mu W$ per $1024^2$.

Further author information:
E-mail: craig.mcmurtry@rochester.edu
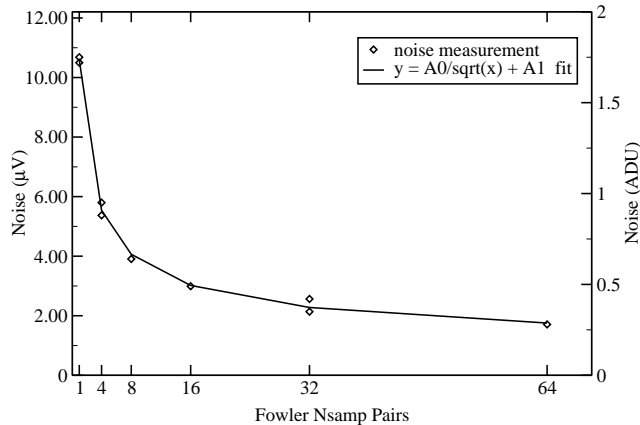
**Figure 1.** Plot of noise versus Fowler sample pairs for the UR system electronics with signal inputs shorted. The overlaid fit uses $y = A0/\sqrt{N} + A1$, where A0 is the normalization/slope, and A1 is the lower noise limit of 0.0808 ADU = 0.493 $\mu$V.

  8. Frame read time $< 12$ seconds per $2048^2$,

The omission of dark current as a requirement is not an over-sight, since the NASA NGST specifications focus on the total noise which includes any noise contribution from the dark current.

    Raytheon Infrared Operations has produced devices for compliance with NGST's requirements. We provide results for Raytheon's SB-226, which is a $1024 \times 1024$ pixel multiplexer. There were two main phases to the testing of the SB-226: Read-Out Integrated Circuit (ROIC) or bare multiplexer (mux) and InSb Sensor Chip Assembly (SCA, InSb bump-bonded to ROIC).

    The first phase of testing involved ROIC evaluations. Since the ROIC is the dominant source of noise voltage, the initial measurements of noise were conducted using bare ROICs to compliment Raytheon's investment in time and resources to develop cryogenic low noise multiplexers. Those noise measurements were then extrapolated to that expected for an InSb SCA by multiplying by a factor of two the ROIC noise in electrons, owing to an estimated doubled nodal capacitance with InSb. As we will show later, the above assumptions proved to be not entirely true, yet provided sufficiently valid results for comparing ROIC noise measurements to InSb SCA noise measurements. Unless otherwise stated, all data were taken using Fowler sampling techniques,[10] where an N Fowler sample pair image is created by subtracting N averaged frame read-outs at the beginning of integration from N averaged frame read-outs at the end of integration. The ROICs' noise data were obtained at 10 seconds integration for 1, 8 and 32 Fowler sample pairs over a temperature range of at least 6 - 80 Kelvin. The noise measurements were obtained using the standard deviation divided by $\sqrt{2}$ in $50 \times 50$ pixel sub-arrays of a difference image made by subtracting two N Fowler sample pair images, i.e. input referred box averaged noise measurement. For NASA's NGST, the noise budget allocates a total of 10 electrons noise for the NIR array and controlling electronics, where $9e^-$ noise is that allowed for the NIR array.[9] For this reason, we have made a noise measurement of the University of Rochester system electronics using shorted inputs (see Figure 1). The University of Rochester system electronics signal chain uses differential amplifiers with input bandwidth limiting at 160 kHz from a single-pole RC filter prior to digitization. Where applicable, we will quote a total noise measurement as well as the derived NIR array noise. The University of Rochester used a pixel read rate of $10\mu s$ per 4 pixels (4 output ROIC). For calibration purposes, the source follower voltage gain and nodal capacitance were measured for each ROIC. The output voltage was monitored as the input bias voltage $V_{dduc}$

**Table 1.** Input referred box averaged per pixel noise measurements for $1024 \times 1024$ SB-226 ROICs taken at 30K using the listed integration times and Fowler sample pairs. Total noise measurements include our system noise, and thus, are real, achievable results. ROIC noise data are derived after subtracting in quadrature the system noise at 32 Fowler sample pairs (0.39 ADU $\times$ ROIC conversion factor).

| ROIC SB226 | 8-Fowler Total Noise 10 s ($e^-$) | 32-Fowler Total Noise 10 s ($e^-$) | 32-Fowler ROIC Noise 10 s ($e^-$) | 32-Fowler Total Noise 1000 s ($e^-$) |
|---|---|---|---|---|
| 1-19-B3 | 6.94 | 3.97 | 3.94 | |
| 1-15-E1 | 6.11 | 3.24 | 3.21 | |
| 2-4-E5 | 6.93 | 3.47 | 3.44 | |
| 2-1-C3 | 6.43 | 3.15 | 3.13 | |
| 1-21-B3 | 5.20 | 2.66 | 2.61 | |
| 1-5-E3 | 7.16 | 3.70 | 3.67 | 3.82 |
| 1-5-E1 | 7.60 | 3.93 | 3.90 | |
| 1-23-B5 | 4.07 | 2.24 | 2.19 | |
| 1-8-C7 | 6.73 | 3.31 | 3.29 | 3.26 |

was varied to produce a source follower voltage gain curve. The capacitance and electron conversion factor were computed using the signal versus noise squared method.[11]

While the first phase of testing gave an indication of Raytheon's ability to produce devices that meet the NGST noise requirement for a multiply sampled 1000 seconds integration, the real verification can only be obtained by direct measurement under conditions specified by M$^c$Creight *et al.*[9] Calibration of the InSb SCA was performed by measuring the source follower voltage gain and capacitance, as described above for the ROIC. The second phase of testing involved InSb SCAs to evaluate well depth, power dissipation, dark current, and multiplexer glow, with associated noises for the latter two. During dark current and multiplexer glow measurements, the bias current supply, $I_{idle}$, on InSb SCAs was evaluated to determine its influence on multiplexer glow, noise, and frame read time. The bias current supply, $I_{idle}$, controls the unit cell current for all the columns in the selected row. We have found that $I_{idle}$ causes unacceptably large multiplexer glow. Fortunately, $I_{idle}$ is not required for operation of these devices. The bias current supply, $I_{slew}$, supplies unit cell current for the 4 columns being read plus the next 4 columns in the selected row. $I_{slew}$ is necessary for operation of the ROIC.

## 2. DATA

### 2.1. ROIC data

Multiple ROICs, representative of the lot splits provided by Raytheon, were tested from January 2001 to May 2001 (see Table 1). Typical source follower gains were measured to be 0.93, for the various lot splits tested. Capacitances for the bare multiplexers averaged around 25fF. Noise measurements were made over broad temperature ranges, 5K to 80K. However, the data listed here are restricted to the relevant temperature of 30K.

The method of box averages for noise measurements allows for more detailed spatial analysis on sub-array scales and is less computationally intensive for the test operator. For a $50 \times 50$ pixel box size, the error in a given measurement is $(\sqrt{(50 \times 50)})^{-1} = 2\%$. For completeness, we have also made a Gaussian fit to a histogram of all of the pixels in a difference image (see Figure 2). The noise measurements were taken using ROIC SB226-1-8-C7 over two 1000 seconds integration at 32 Fowler sample pairs. The standard deviation derived from this Gaussian fit is $4.61e^-$, which gives a total frame input referred box average noise of $4.61e^-/\sqrt{2} = 3.26e^-$, in good agreement with the noise reported for 10 seconds in Table 1. Figure 2 shows an offset or non-zero mean of $-38e^-$ which is caused by a drift of the ROIC's output as the temperature drifted over 0.5K during the total 2000 seconds of integration for the two images. However, this drift in temperature, remarkably, did not cause an increase in noise.
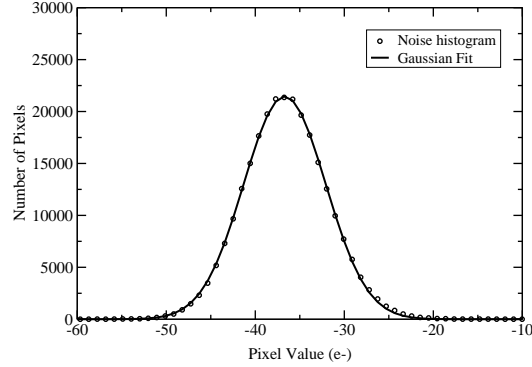
**Figure 2.** Histogram of pixel values from a 1000 seconds integration difference frame of $511 \times 512 = 261632$ pixels for SB226-1-8-C7. The overlaid fit is a Gaussian fit using $y = A0e^{-0.5(x-A2)^2/A1^2}$, where A0 is the normalization, A1 is the standard deviation and A2 is the mean.

## 2.2. InSb SCA data

InSb SCA 416431, SB-226-1-18-E3 was tested extensively between June 2001 and February 2002. As stated earlier, the SB-226 ROIC is a pathfinder multiplexer, and Raytheon did not select either the best ROIC from the SB-226 lot splits or the best (optimized for lowest dark current) InSb wafer material for this SCA. The ROIC used for SCA 416431 was based on the same design and processing as ROIC 1-8-C7, which had $3.29e^-$ total noise in 10 seconds 32 Fowler sample pairs. The best SB-226 ROIC had $2.19e^-$ total noise for the same situation (see Table 1). As such, the data represent milestones achieved for the NGST specifications and requirements, but is not a limit to what Raytheon and University of Rochester have accomplished. The source follower gain for SCA 416431 is 0.97 as determined from the $V_{dduc}$ voltage versus $V_{out}$ voltage curve. The mean pixel capacitance was measured to be 88fF. Noise and dark current data were obtained for temperatures between 30K and 50K (data discussed below). A mean well depth of $350 \pm 10$ mV, equivalent to $1.8 \times 10^5 e^-$, at 500mV applied bias was measured. Power dissipation was calculated from current and voltage measurements for the unit cell and signal chain of the multiplexer. Power dissipation from SCA 416431 is $400\mu$W using $I_{idle}$, $110\mu$W without $I_{idle}$ during normal read-out or integration and $650\mu$W without $I_{idle}$ during reset, which is negligible compared to the time of read-out or integration. Although pixel operability can not be stated without strict adherence to all the NGST requirements, we can state that SCA 416431 does show preliminary pixel operability of $> 99\%$. The quantum efficiency was measured using room temperature blackbody radiation. The mean quantum efficiency at $3.27\mu$m is 94.8% with a pixel-to-pixel variation of $\pm 1.6\%$.

Initial dark current, noise and bias $I_{idle}$ testing were performed on InSb SCA 416431, SB-226-1-18-E3, reading out sub-arrays of $511 \times 512$ and $1024 \times 252$. The image data were obtained using multiple sampling (32 Fowler sample pairs) at various integration times (25, 50, 100, 200, 350, 500, 750, and 1000 seconds). Each integration time was repeated a total of three times (except for the shortest integration time) to reduce the likelihood of contaminated data and to demonstrate repeatability. These sets of data were obtained for four cases: array size $511 \times 512$ with $I_{idle} = 0\mu$A; $511 \times 512$ with $I_{idle} = 100\mu$A; $1024 \times 252$ with $I_{idle} = 100\mu$A; and $1024 \times 252$ with $I_{idle} = 0\mu$A. The dark charge was measured in $50 \times 50$ pixel box averages at various locations on the array (See Table 2). Hot pixels and cosmic ray hits were removed by rejecting pixels that were more than four standard deviations away from the median value. Rejected pixels amounted to less than 1% (see pixel operability above), even at the longest integrations where there were a high number of cosmic ray events. A line was then fit to dark charge versus integration time for the longer integrations in the region of linear growth (see Figure 3). The resultant slope is the dark current and is listed in Table 2. We anticipate considerably lower dark currents on candidate NGST arrays, because better materials and passivation techniques will be employed.
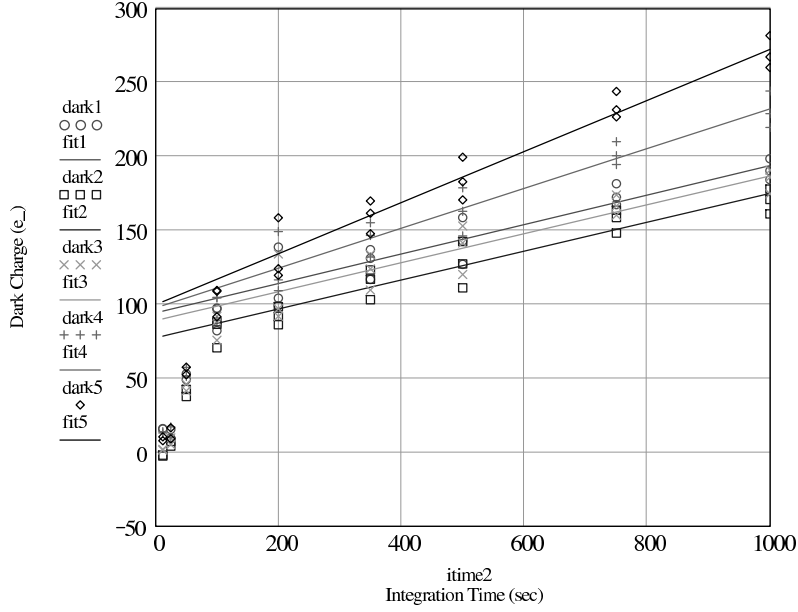
**Figure 3.** Plot of dark charge versus integration time, with linear fits for dark current at integration times > 100 seconds. The data represent the five regions of Case D in Table 2

**Table 2.** The data were taken at T = 30.0K. Values are per pixel. Case A and B are array size 511 rows by 512 columns. Case C and D are 1024 rows by 252 columns. Noise measurements include our system noise, and thus, are real, achievable results. Subtracting in quadrature the electronic system noise, $0.39\text{ADU} \times 3.2e^-/\text{ADU} = 1.25e^-$, produces, at best, a noise that is lower by $0.07e^-$. The Dark Charge at 0 seconds is extrapolated from the dark current line fit (y-intercept). The Dark Signal at 1000 seconds is the total average pixel value in the given region.

| $I_{idle}$ ($\mu A$) | Region | Dark Current ($e^-$/sec) | Dark Charge @ 0s ($e^-$) | Dark Signal @ 1000s ($e^-$) | Noise 32-Fow @ 1000s ($e^-$) |
|---|---|---|---|---|---|
| 0 | 51:100,51:100 | 0.103 | 55.9 | 154 | $11.35 \pm 0.08$ |
| (case A) | 71:120,231:280 | 0.101 | 45.0 | 144 | $11.39 \pm 0.22$ |
| | 71:120,431:480 | 0.113 | 48.3 | 160 | $11.35 \pm 0.15$ |
| 100 | 51:100,51:100 | 0.432 | 446.6 | 868 | $17.03 \pm 0.11$ |
| (case B) | 71:120,231:280 | 0.399 | 422.1 | 811 | $16.57 \pm 0.20$ |
| | 71:120,431:480 | 0.404 | 457.9 | 842 | $17.14 \pm 0.07$ |
| 100 | 51:100,51:100 | 0.412 | 498.8 | 900 | $16.79 \pm 0.03$ |
| (case C) | 71:120,231:280 | 0.382 | 444.9 | 815 | $16.71 \pm 0.09$ |
| | 71:120,431:480 | 0.422 | 470.0 | 882 | $17.22 \pm 0.22$ |
| | 71:120,701:750 | 0.527 | 569.1 | 1083 | $18.97 \pm 0.21$ |
| | 71:120,901:950 | 0.638 | 627.8 | 1253 | $20.18 \pm 0.10$ |
| 0 | 51:100,51:100 | 0.100 | 99.3 | 191 | $11.41 \pm 0.11$ |
| (case D) | 71:120,231:280 | 0.098 | 77.5 | 166 | $10.83 \pm 0.19$ |
| | 71:120,431:480 | 0.098 | 89.1 | 181 | $11.51 \pm 0.12$ |
| | 71:120,701:750 | 0.135 | 97.7 | 227 | $12.31 \pm 0.18$ |
| | 71:120,901:950 | 0.173 | 99.8 | 269 | $13.63 \pm 0.18$ |

The noise data in Table 2 were derived from the three 1000 seconds integration (32 Fowler sample pairs) images. A single 1000 seconds image was subtracted from a second 1000 seconds image to produce a difference image. This resulted in three distinct difference images from the three 1000 seconds integration images. The noise measurements were obtained from the standard deviation of the difference images divided by $\sqrt{2}$, using $50 \times 50$ pixel sub-arrays, i.e. input referred box average noise measurement, with hot pixels and cosmic ray hits rejected as mentioned above. Pixels that did not respond to light or dark current were also removed to avoid skewing the noise measurement with artificial zero value pixels (recall that the noise difference image has a typical mean near zero). Again, the total number of rejected pixels amounted to less than 1% of the total pixels used. For a given sub-array location, each of these three noise measurements was then averaged to the single value represented in Table 2. Note that these noise measurements are total noise measurements for the 1000 seconds integration and include noise from the multiplexer or read noise, noise from dark current, our electronic systems and other sources. A few of the noise measurements come close to the NGST total noise requirement of 9 $e^-$ (10 including system noise) for a 1000 seconds integration, even though Raytheon did not use the best InSb.

Further tests of $I_{idle}$ as well as $I_{slew}$ and reset clock levels (pReset) were performed on InSb SCA 416431 using the full array size, $1024 \times 1024$ (see Table 3). The three parameters were varied to determine their effect on both dark current and noise. The two bias current supplies were set at different levels. $I_{idle}$ was set to $100\mu$A or $0\mu$A (off). $I_{slew}$ was set to $12\mu$A or $6\mu$A, but could not be entirely turned off since it supplies the pixel slew current. The reset clock off and on voltage levels were adjusted from nominal ($-3.1$V = on, $-5.5$V = off) to optimized levels derived by subtracting 0.5V from $V_{dduc}$ for the on voltage level and subtracting 1.5V from $V_{dduc}$ for the off voltage level ($-4.1$V = on, $-5.1$V = off). As with the initial $I_{idle}$ testing on sub-arrays, the image data were obtained using multiple sampling (32 Fowler sample pairs) at various integration times (25, 50, 100, 200, 350, 500, 750, and 1000 seconds). Each integration time was repeated a total of three times (except for the 1000 seconds integration time which was repeated four times) to reduce the likelihood of contaminated data and to show repeatability. Pixel rejection was performed as mentioned above. Noise data were also derived in the same manner as previously mentioned.

## 3. ANALYSIS

As mentioned in Section 1, the University of Rochester and Raytheon evaluated bare ROICs for initial NGST testing, and scaled the noise results based on assumed doubling of capacitances between ROIC and InSb SCA. Upon evaluating InSb SCAs, it was found that the capacitances increased by factors of three or slightly more above the capacitance of a bare ROIC, while the measured InSb SCA noises only increased by factors between 2.3 and 2.6 above the bare ROIC read noise.

The most obvious feature of the above data is that the current source, $I_{idle}$, adds significantly to both the noise and the dark current. By comparing Cases B and C, where $I_{idle} = 100\mu$A, to Cases A and D, where $I_{idle} = 0\mu$A, one sees that when $I_{idle}$ is used there is four times the dark current and the noise rises.

For Case C and Case D, there was significant glow from the last row which was left enabled during integration (see Figure 4). The larger amount of glow from the last row occurs when $I_{idle} = 100\mu$A (Case B and C). However, for all four cases, the last eight pixels (columns) are also enabled and thus receive $I_{slew} = 8\mu$A, which in turn manifests as a glow that is semi-point like and centered at the last eight pixels (top right in Figure 4). The last row glow does contribute to the total noise and is consistent with shot noise. Taking the dark current with glow (at 71:120,901:950) and subtracting the dark current without glow (at 71:120,231:280) over the total integration to yield a dark charge of:

$$(0.173e^-/\text{sec} - 0.098e^-/\text{sec}) \times 1000\text{sec} = 75e^-, \tag{1}$$

where the expected noise (shot) due to this dark charge should be the square root of this dark charge. Adding in quadrature the result to the noise in the region without glow gives:

$$\sqrt{(10.83)^2 + 75} = 13.87e^-, \tag{2}$$

which is nearly identical to the noise obtained directly for the same region affected by the last row glow. All three array sizes used in Tables 2 and 3 and the corresponding dark current show a trend relating to the

**Table 3.** The data were taken at T = 30.0K with array size 1024 × 1024. Values are per pixel. Noise measurements include our system noise, and thus, are real, achievable results. Subtracting in quadrature the electronic system noise, $0.39\text{ADU} \times 3.2e^-/\text{ADU} = 1.25e^-$, produces, at best, a noise that is lower by $0.07e^-$. The Dark Charge at 0 seconds is extrapolated from the dark current line fit (i.e. y-intercept). The Dark Signal at 1000 seconds is the total average pixel value in the given region.

| $I_{idle}$ ($\mu A$) | $I_{slew}$ ($\mu A$) | pReset | Region | Dark Current ($e^-$/sec) | Dark Charge @ 0s ($e^-$) | Dark Signal @ 1000s ($e^-$) | Noise 32-Fow @ 1000s ($e^-$) |
|---|---|---|---|---|---|---|---|
| 100 | 12 | nominal | 51:100,51:100 | 0.323 | 207.6 | 522 | 14.35 ± 0.17 |
| (case 1) | | | 71:120,231:280 | 0.337 | 185.8 | 518 | 16.66 ± 1.75 |
| | | | 71:120,431:480 | 0.337 | 207.2 | 534 | 16.85 ± 1.29 |
| | | | 71:120,701:750 | 0.419 | 261.6 | 669 | 17.59 ± 0.10 |
| | | | 71:120,901:950 | 0.503 | 289.6 | 780 | 19.30 ± 0.20 |
| | | | 601:650,81:130 | 1.229 | 194.4 | 1418 | 29.83 ± 1.01 |
| 0 | 12 | nominal | 51:100,51:100 | 0.073 | 16.5 | 129 | 10.11 ± 0.19 |
| (case 2) | | | 71:120,231:280 | 0.068 | 14.3 | 125 | 9.89 ± 0.23 |
| | | | 71:120,431:480 | 0.076 | 13.9 | 131 | 10.39 ± 0.26 |
| | | | 71:120,701:750 | 0.089 | 16.5 | 154 | 11.12 ± 0.16 |
| | | | 71:120,901:950 | 0.113 | 17.1 | 180 | 12.09 ± 0.14 |
| | | | 601:650,81:130 | 0.393 | 12.3 | 457 | 16.47 ± 0.20 |
| 0 | 12 | optimized | 51:100,51:100 | 0.098 | 89.0 | 182 | 12.88 ± 0.27 |
| (case 3) | | | 71:120,231:280 | 0.080 | 83.1 | 157 | 12.14 ± 0.18 |
| | | | 71:120,431:480 | 0.096 | 87.0 | 176 | 12.85 ± 0.15 |
| | | | 71:120,701:750 | 0.148 | 96.5 | 237 | 14.76 ± 0.14 |
| | | | 71:120,901:950 | 0.211 | 94.9 | 301 | 16.94 ± 0.30 |
| | | | 601:650,81:130 | 0.979 | 65.8 | 1040 | 27.80 ± 0.70 |
| 0 | 6 | optimized | 51:100,51:100 | 0.204 | 67.0 | 262 | 12.85 ± 0.14 |
| (case 4) | | | 71:120,231:280 | 0.187 | 59.4 | 240 | 12.45 ± 0.19 |
| | | | 71:120,431:480 | 0.201 | 71.4 | 263 | 13.41 ± 0.11 |
| | | | 71:120,701:750 | 0.263 | 80.9 | 336 | 15.21 ± 0.16 |
| | | | 71:120,901:950 | 0.331 | 82.1 | 403 | 17.08 ± 0.36 |
| | | | 601:650,81:130 | 1.110 | 59.9 | 1162 | 27.92 ± 0.76 |
| 0 | 6 | nominal | 51:100,51:100 | 0.098 | 33.8 | 128 | 10.20 ± 0.24 |
| (case 5) | | | 71:120,231:280 | 0.092 | 29.5 | 118 | 10.10 ± 0.13 |
| | | | 71:120,431:480 | 0.098 | 31.9 | 128 | 10.72 ± 0.15 |
| | | | 71:120,701:750 | 0.125 | 37.5 | 160 | 11.57 ± 0.14 |
| | | | 71:120,901:950 | 0.154 | 37.5 | 189 | 12.33 ± 0.25 |
| | | | 601:650,81:130 | 0.475 | 26.4 | 499 | 17.04 ± 0.20 |
| 100 | 12 | optimized | 51:100,51:100 | 0.506 | 246 | 739 | 18.91 ± 0.32 |
| (case 6) | | | 71:120,231:280 | 0.466 | 243 | 704 | 17.42 ± 0.30 |
| | | | 71:120,431:480 | 0.507 | 254 | 752 | 19.97 ± 0.62 |
| | | | 71:120,701:750 | 0.645 | 312 | 944 | 22.61 ± 0.38 |
| | | | 71:120,901:950 | 0.816 | 354 | 1158 | 28.41 ± 1.38 |
| | | | 601:650,81:130 | 2.531 | 246 | 2771 | 48.33 ± 2.32 |
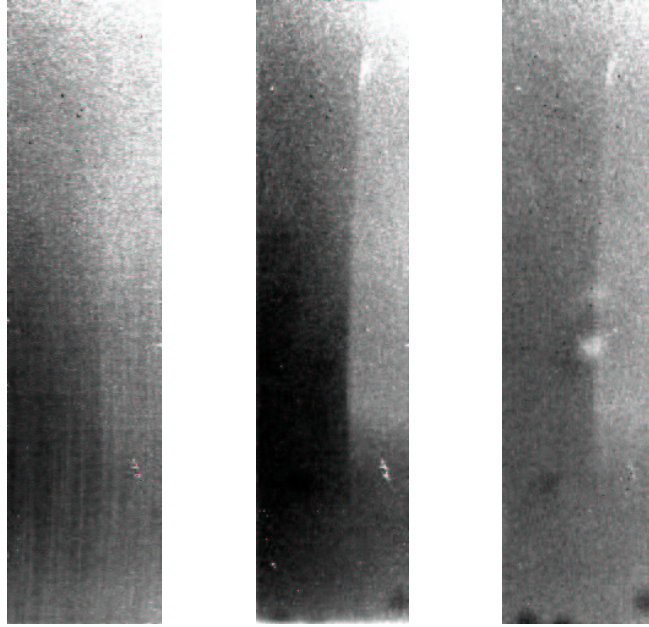
**Figure 4.** Images of sub-array size $252 \times 1024$ showing dark charge and last row glow (top). Pixel 1,1 is in lower left corner. All three images were taken using Fowler sampling with 32 sample pairs. Left image is a 1000 seconds integration with $I_{idle} = 100\mu A$. Middle image is a 1000 seconds integration with $I_{idle} = 0\mu A$. Right image is a dark current plus glow map made by subtracting a 500 seconds integration from 1000 seconds integration with $I_{idle} = 0\mu A$. On the right hand side of the images, a light leak can be seen, but this is blocked for the left side where dark current measurements were made. Most of the cosmic ray hits and bad pixels have been filtered from the images. The right image also shows anomalous "black holes" both in positive and negative. The images are not scaled to the same intensity levels.

proximity of a given region to both the last row and last four columns, where glow originates from $I_{idle}$ and $I_{slew}$, respectively (see Figure 4). These glows can be reduced or eliminated by turning off $I_{idle}$, and disabling or de-selecting both the last row and the last four columns during integration. It is believed that elimination of glows from $I_{idle}$ and $I_{slew}$ would produce more uniform noise results at the lowest achieved level, $9.89e^-$, across the entire InSb array.

Between 0 and 100 seconds, there is a dark charge-up or settling time charge (see Figure 3, short integration charge ramp-up). The settling time charge is different for each case that we investigated. However, this settling time charge does not contribute to the noise.

The charge associated with dark current itself does not completely follow Poisson statistics since the added noise is below what one would expect for shot noise. Specifically, we will focus on the data for $I_{idle} = 0\mu A$ (Case D) in the region 71:120,231:280. Input referred box average noise measurements, obtained at 1000 seconds integration and 32 Fowler sample pairs from a bare multiplexer (ROIC), indicate a total noise of $3.19e^-$. The input nodal capacitance of an InSb SCA is significantly larger than that of a bare multiplexer. However, scaling the bare multiplexer noise with ROIC capacitance to the expected noise for a larger nodal capacitance InSb SCA is not valid as determined in our ROIC and SCA testing. Data obtained at 10 seconds integration and 32 Fowler sample pairs showed a total noise of $3.07e^-$ for a bare ROIC and $8.20e^-$ for the same InSb SCA, which should be read noise dominated at short integration times. Therefore, we use data obtained from an ROIC at both 10 and 1000 seconds integration to scale 10 seconds integration noise data for InSb SCA to the longer, 1000 seconds integration time:

$$8.20e^- \times \frac{3.19e^-}{3.07e^-} = 8.52e^-. \tag{3}$$

The dark charge due to dark current at the end of 1000 seconds integration is:

$$0.098e^-/\text{sec} \times 1000\text{sec} = 98e^-, \tag{4}$$

where the expected noise due to this dark charge should be the square root of this dark charge. Adding in quadrature the scaled ROIC read noise to the shot noise expected for dark current gives a total noise of:

$$\sqrt{(8.52)^2 + 98} = 13.1e^-, \tag{5}$$

which is significantly larger than the measured $10.83e^-$. Even without scaling the $8.20e^-$ (Equation 3) InSb SCA noise at 10 seconds integration and 32 Fowler sample pairs, the quadrature summed noise is still greater than the measured noise ($10.83e^-$):

$$\sqrt{(8.20)^2 + 98} = 12.9e^-. \tag{6}$$

Now, if we use $8.52e^-$ (Equation 3) as the total ROIC noise and subtract in quadrature from the total SCA measured noise:

$$10.83^2 - 8.52^2 = 44.70, \tag{7}$$

then we obtain the total dark charge that follows shot noise statistics. This would translate to $0.0447e^-/sec$ dark current at 30K, which is reasonably consistent with data obtained between 38K and 50K (see Figure 5). An Arrhenius plot was made from dark current data taken between 38K and 50K and the dark current from Table 3 at 30K (see Figure 5). The Arrhenius plot also shows the predicted dark current from diffusion and generation-recombination processes[12,13,14] compared with measured data.

Similar arguments regarding noise statistics and dark current apply to the data in Table 3 for $1024 \times 1024$ array size. Table 3 shows that the dark currents are related to pReset clock values. The trend shows larger dark currents when optimized reset voltages are used versus nominal reset voltages. The optimized reset voltages give a slightly larger actual bias across the detector. It is believed that this is an indication that dark current due to tunneling processes are involved for the moderate quality InSb used in SCA 416431. At this time, we have not fully investigated this hypothesis, and will investigate this phenomenon if it is seen in the next generation, higher quality InSb array detectors.

## 4. CONCLUSIONS

InSb SCA 416431 has achieved $\sim 10e^-$ total noise in 1000 seconds multiply sampled integration, $\sim 95\%$ quantum efficiency (near NGST goal), well depths $> 1.8 \times 10^5 e^-$ (near goal), pixel operability $> 99\%$ (near goal), frame read time $< 3$ seconds per $1024^2$ pixels, and power dissipation $\sim 110\mu$W (near goal) at 30K. Dark current is only important with regards to its contribution to the total noise, as specified by the NGST requirements. These results for the pathfinder SB-226 InSb SCA 416431 (recall ROIC and InSb for this SCA were not the best produced, see Section 2.2) show that Raytheon has produced array detectors that meet or exceed most of the stringent requirements of NGST (see Section 1 and M$^c$Creight *et al.*[9]) and, impressively, approach several of the goals. Raytheon's next generation ROIC, SB-304 (array format $2048 \times 2048$, see Raytheon companion paper, these SPIE proceedings), with refined InSb wafer material, is expected to exceed the NGST requirements and meet many of the goals. Given past achievements and the results presented here, Raytheon InSb detector arrays are an excellent choice for high sensitivity, low background and low noise applications in the 1 to 5 $\mu$m region both for ground-based instruments and space-borne missions.

## ACKNOWLEDGMENTS
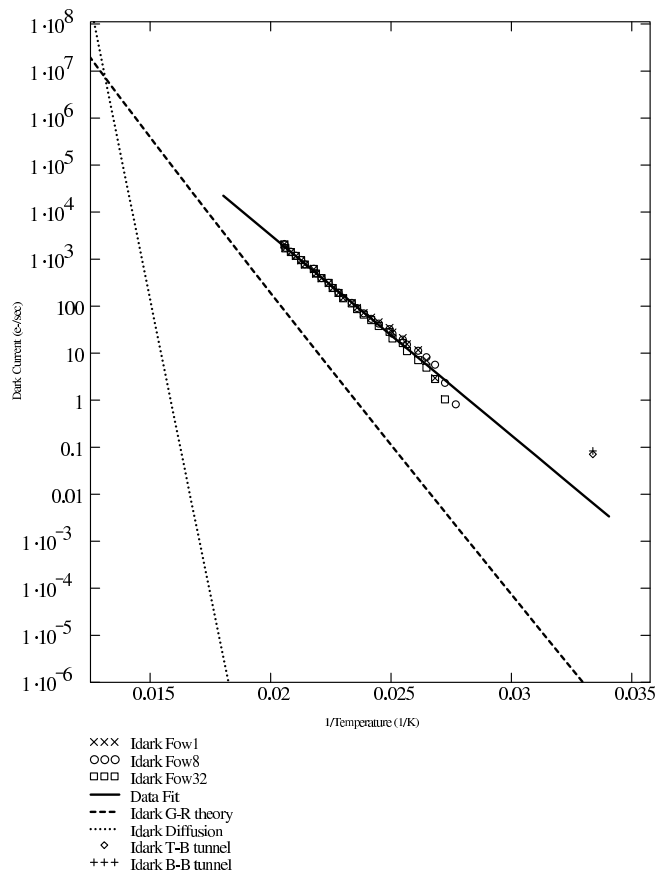
**Figure 5.** Plot of dark current versus inverse temperature, with a fit to the data. Plots of dark current theory for diffusion, and generation-recombination processes are included.

## REFERENCES

1. W. J. Forrest, "Next Generation Space Telescope Instrument Technology Developement," *Proposal to NASA NRA 00-OSS-03*, 2000.

2. J. Wu, W. J. Forrest, J. L. Pipher, N. Lum, and A. Hoffman, "Development of infrared focal plane arrays for space," *Review of Scientific Instruments* **68**, pp. 3566–3578, Sept. 1997.

3. J. L. Hora, G. G. Fazio, S. P. Willner, M. L. Ashby, J. Huang, S. T. Megeath, J. R. Stauffer, E. V. Tollestrup, Z. Wang, W. J. Glaccum, J. L. Pipher, W. J. Forrest, C. R. McCreight, M. E. McKelvey, W. F. Hoffman, P. Eisenhardt, J. A. Surace, W. T. Reach, S. H. Moseley, R. G. Arendt, K. P. Stewart, and F. D. Robinson, "Calibration and performance of the infrared array camera (IRAC)," in *Proc. SPIE, Infrared Spaceborne Remote Sensing VIII,*, M. Strojnik and B. F. Andresen, eds., **4131**, pp. 13–25, Nov. 2000.

4. W. J. Forrest, H. Chen, J. D. Garnett, S. L. Solomon, and J. L. Pipher, "Near-infrared arrays for SIRTF, the Space Infrared Telescope Facility," in *Proc. SPIE, Infrared Detectors and Instrumentation,*, A. M. Fowler, ed., **1946**, pp. 18–24, Oct. 1993.

5. J. D. Garnett and W. J. Forrest, "Multiply sampled read-limited and background-limited noise performance," in *Proc. SPIE, Infrared Detectors and Instrumentation,*, A. M. Fowler, ed., **1946**, pp. 395–404, Oct. 1993.

6. A. W. Hoffman, K. J. Ando, A. D. Estrada, J. D. Garnett, N. A. Lum, P. J. Love, J. P. Rosbeck, K. P. Sparkman, A. M. Fowler, J. L. Pipher, and W. J. Forrest, "Near IR arrays for ground-based and space-based

astronomy," in *Proc. SPIE, Infrared Astronomical Instrumentation,*, A. M. Fowler, ed., **3354**, pp. 24–29, Aug. 1998.

7. G. G. Fazio, J. L. Hora, S. P. Willner, J. R. Stauffer, M. L. Ashby, Z. Wang, E. V. Tollestrup, J. L. Pipher, W. J. Forrest, C. R. McCreight, S. H. Moseley, W. F. Hoffmann, P. Eisenhardt, and E. L. Wright, "Infrared array camera (IRAC) for the Space Infrared Telescope Facility (SIRTF)," in *Proc. SPIE, Infrared Astronomical Instrumentation,*, A. M. Fowler, ed., **3354**, pp. 1024–1031, Aug. 1998.

8. J. L. Pipher, W. J. Forrest, and J. Wu, "InSb arrays for SIRTF," in *Proc. SPIE, Infrared Detectors and Instrumentation for Astronomy,*, A. M. Fowler, ed., **2475**, pp. 428–434, June 1995.

9. C. M<sup>c</sup>Creight, M. Greenhouse, D. Figer, R. Martineau, M. Jurotich, and B. Seery, "NGST ISIM Technology Development Requirements and Goals for NGST Detectors," *http://www.ngst.nasa.gov/doclist/bytitle.html* **Document 641**, 2001.

10. A. M. Fowler and I. Gatley, "Noise reduction strategy for hybrid IR focal-plane arrays," in *Proc. SPIE, Infrared Sensors: Detectors, Electronics, and Signal Processing,*, T. S. Jayadev, ed., **1541**, pp. 127–133, Nov. 1991.

11. L. Mortara and A. Fowler, "Evaluations of CCD: Performance for Astronomical Use," *Proc. SPIE, Solid State Imagers for Astronomy* **290**, pp. 28–30, 1981.

12. R. D. Thom and B. T. Yang, "Low-background InSb array development," in *NASA. Ames Research Center Proceedings of the Second Infrared Detector Technology Workshop (SEE N87-13704 05-35)*, Feb. 1986.

13. W. Shockley and W. T. Read, Jr., "Statisics of the Recombinations of Holes and Electrons," *Phys. Rev.* **87**, pp. 835–842, 1952.

14. R. N. Hall, "Electron-Hole Recombination in Germanium," *Phys. Rev.* **87**, p. 387, 1952.